Optical generation, templating, and polymerization of three-dimensional arrays of liquid-crystal defects decorated by plasmonic nanoparticles

Julian S. Evans,[1] Paul J. Ackerman,[1,2,3] Dirk J. Broer,[4] Jao van de Lagemaat,[1,3,5] and Ivan I. Smalyukh[1,2,5,*]

[1]*Department of Physics and Materials Science and Engineering Program, University of Colorado at Boulder, Boulder, Colorado 80309, USA*

[2]*Department of Electrical, Computer, and Energy Engineering and Liquid Crystals Materials Research Center, University of Colorado at Boulder, Boulder, Colorado 80309, USA*

[3]*National Renewable Energy Laboratory, Golden, Colorado 80401, USA*

[4]*Functional Organic Materials and Devices, Eindhoven University of Technology, Box 513, 5600 MB Eindhoven, The Netherlands*

[5]*Renewable and Sustainable Energy Institute, National Renewable Energy Laboratory and University of Colorado at Boulder, Boulder, Colorado 80309, USA*

(Received 31 December 2012; published 12 March 2013)

Defects in liquid crystals are used to model topological entities ranging from Skyrmions in high-energy physics to early-universe cosmic strings, as well as find practical applications in self-assembly of diffraction gratings and in scaffolding of plasmonic nanoparticles, but they are hard to control and organize into three-dimensional lattices. We laterally scan focused laser beams to produce periodic arrays of twist-stabilized defects forming either linear (fingers) or axially symmetric (torons) configurations in partially polymerizable liquid crystal films. Polymerization allows for stabilization of these structures and the formation of three-dimensional arrays of defects by stacking of the thin cholesteric films on top of each other. In the process of fabrication of such arrays, we polymerize the liquid crystal film with an array of torons or fingers and then sequentially produce and photopolymerize new liquid crystal layers on top of it, thus obtaining a three-dimensional structure of twist-stabilized defects in a layer-by-layer fashion. Templating by the polymerized layer spontaneously yields ordered organization of fingers and torons in the new cholesteric layer, thus enabling a three-dimensional ordered structure of defects. Nondestructive three-dimensional imaging of director fields by use of three-photon excitation fluorescence polarizing microscopy reveals the nature of topological singularities and physical underpinnings behind the observed templating effect. Three-dimensional patterning of defects templates the self-assembly of plasmonic nanoparticles into individual singularities and their arrays, laying the groundwork for potential applications in nanophotonics, plasmonics, metamaterial fabrication, and nanoscale energy conversion.

DOI: 10.1103/PhysRevE.87.032503 PACS number(s): 61.30.Hn, 61.30.Jf, 61.25.hp

I. INTRODUCTION

Topological defects in liquid crystals (LCs) provide optically imagable models of Skyrmions first introduced in particle physics [1] and recently also observed in chiral magnets [2,3], phase singularities found in electron [4,5] and laser beams [6,7], and early-universe cosmic strings [8]. In addition to regular point, line, and wall defects, LCs can support the existence of director fields in the form of Hopf fibrations, torons, merons, Skyrmions [9–14], and linked and knotted disclination loops [15] stabilized by chirality, colloids, or both. Arrays of line defects enable the realization of thermodynamically stable twist grain boundary and blue phases of LCs, in which periodic arrangements of defects are found in the ground state [16]. Optical anisotropy of the LC enables a large number of potential applications, such as diffraction gratings and optical vortex generators [13,14], as well as experimental exploration of low-dimensional topology [17]. However, generation and stabilization of three-dimensional patterns of these defects in LCs is nontrivial and has not been achieved so far.

When a cholesteric LC is confined in a homeotropic cell with thickness on the order of the equilibrium cholesteric pitch, the system is frustrated and either remains in a purely unwound homeotropic state or forms well-defined, isolated, solitonic defects known as fingers and torons [10–14,18,19], which allow for local twisting of the LC director field $\mathbf{n}(\mathbf{r})$ to occur. The torons of the first type consist of two hyperbolic hedgehog point defects and a looped double-twist cylinder that introduces energetically favorable twist while satisfying the boundary conditions set by the confining substrates and matching the vertically aligned far-field director $\mathbf{n}_0$ [10]. Torons can also mediate an experimental realization of the Hopf fibration, which plays an important role in topology and is also found in toroidal DNA condensation [9,17,20]. Fingers of the first type resemble merons in various other condensed matter systems [21]. Similar to the so-called Lehmann clusters observed in short-pitch cholesterics [22–24], they consist of twist-stabilized quadrupoles of λ disclinations of half-integer strengths with translational invariance along their length. Although these defects are long-term stable in nonpolymerizable cholesteric LC systems, they can move around in the LC cells due to thermal fluctuations when generated using focused beams of relatively low laser generation power (note that optical generation at high laser powers can mitigate this problem and allow for formation of large periodic arrays) [13]. The torons also can be perturbed during optical imaging as well as when the LC responds to temperature changes, mechanical stresses, and various external fields. Although this facile response of torons, fingers, and their periodic arrays to external fields can be utilized to realize optically and electrically tunable diffraction gratings and optical vortex generators [13,14], some of the potential applications of toron arrays may require thin solid films that are

*ivan.smalyukh@colorado.edu

insensitive to external fields and temperature variations in the surrounding environment. Although photopolymerization is a natural approach to achieve such structured films with arrays of defects, these films have not been experimentally realized so far and only two-dimensional arrays of torons and fingers have been demonstrated in nonpolymerized systems [13,14].

Nanoparticles possess optical and other properties that are often not observable in the bulk materials of the same chemical composition, most notably surface-plasmon resonance in metallic particles [25,26], quantum confinement [27–29] and multiple-exciton generation [29] in semiconductor nanoparticles, and increased chemical activity due to a large surface area to volume ratio and rougher surfaces in a variety of different nano-sized colloids [30]. Over the past several decades, chemists have developed well-controlled syntheses of anisotropic nanocrystal particles with orientation-dependent optical properties (see, for example, Refs. [25–31]). The control of alignment, orientation, and assembly of individual and small groups of such anisotropic nanoparticles is important for understanding their collective behavior for the development of approaches for fabrication of optical metamaterials, plasmonic, nanophotonic, and solar energy harvesting technologies [29–40]. The energetic cost of LC defects allows them to entrap and orient fluid-borne anisotropic nanoparticles in a reproducible manner and with well-controlled position and orientation [31]. However, these particle-defect assemblies can undergo Brownian motion in a fluid LC medium and interact with each other over time. Although these elasticity-mediated interactions can enable hierarchical self-assembly of nanoparticles and defects into colloidal superstructures defined by colloidal microparticles [31], they preclude the possibility of patterning of nanoparticles into arbitrary trap arrays defined by topological defects alone. Furthermore, the typical requirement of working with a fluid cell of thickness comparable to the cholesteric pitch often makes the exploration of three-dimensional interactions and assemblies impossible. Similar to the arrays of defects without nanoparticles, some of the applications of periodic defect-nanoparticle assemblies may benefit from converting them into solid thin films with a "frozen" original structure and composition obtained by means of the optically guided self-assembly of arbitrary arrays of torons and fingers.

In this work, we polymerize the twist-embedding structures of torons and fingers as well as assemble various three-dimensional defect arrays controlled by means of scanned laser beams and soft templating. Producing these arrays in a partially polymerizable system allows for layer-by-layer templated assembly of LC structures and postproduction control of the effective optical anisotropy of the sample (e.g., via washing out most of the unpolymerized LC and subsequent infiltration of the ensuing nanoporous thin films with isotropic fluids). Polymerization stabilizes the obtained three-dimensional defect structures and ensuing $\mathbf{n}(\mathbf{r})$ configurations against mechanical stresses, ambient temperature variations, and external fields (whenever this response is unwanted). Polymerization also eliminates Brownian motion of torons and fingers and makes the presence of confining glass substrates unnecessary, allowing for the generation of multilayer structures with well-defined defect configurations as well as for obtaining thin flexible films with controlled $\mathbf{n}(\mathbf{r})$ and nanoparticle patterns. We demonstrate that, during the multilayer patterning of defects, the thickness variations and director distortions associated with partially polymerized films have an interesting templating effect on the new layer, allowing for exploration of the fundamental physical underpinnings behind these topological structures and being potentially useful for large-scale production. Control of polymerization conditions can lead to the permanent capture of nonequilibrium $\mathbf{n}(\mathbf{r})$ configurations to enable studies of toron formation and unstable nonequilibrium geometries not observed in nonpolymerizable LC systems. Furthermore, our system may allow for detailed fundamental explorations of the interplay between topologies of Hopf fibrations, torons, merons, Skyrmions, and various LC singularities in the form of line and point defects that may have an impact on the understanding of other condensed matter systems. Thus the demonstrated ability of three-dimensional patterning of topological defects in the LC system and nondestructive imaging of the ensuing molecular alignment fields and defects may also enable a fertile ground for new basic science.

II. MATERIALS, METHODS, AND TECHNIQUES

A. Sample preparation

The studied partially polymerizable cholesteric LC mixture was prepared by first mixing 69% of nonreactive nematic E7 with 30% of a diacrylate nematic (consisting of 12% of RM 82 and 18% of RM 257) and 1% initiator Irgacure 184, which was then followed by mixing of 99.8% of this nematic mixture with 0.2% of reactive chiral mesogen LC756 (Fig. 1). The nematic compounds have been obtained from Merck and EM Chemicals. The chiral additive LC756 was obtained from BASF and the photoinitiator from CIBA Specialty Chemicals. The obtained powder mixture was first dissolved in dichloromethane to homogenize, heated to 85 °C for one day to remove the solvent, and cooled down to obtain a room-temperature chiral nematic mixture with the equilibrium cholesteric pitch $p = 9$ μm. This cholesteric mixture was infiltrated into LC cells with homeotropic anchoring boundary conditions and thickness d comparable to p and optimized for stabilization of unwound director configurations at zero field while enabling generation of multistable twisted configurations, such as arrays of fingers and torons. To fabricate the cells, glass substrates with conductive indium tin oxide (ITO) coatings were spin coated with polyimide SE1211 (Nissan) at 2700 rpm for 30 s and then baked (5 min at 90 °C followed by 1 h at 180 °C) to set strong vertical surface boundary conditions for the LC director. Electrically controlled wedge cells with thickness $d = 7$–10 μm were produced by separating two glass substrates with glass fiber segments of diameter 7 μm in UV curable glue at one end of the cell and segments of diameter 10 μm in UV curable glue at the opposite end of the cell. We have infiltrated the LC into the cells by capillary forces in the isotropic phase at 80 °C to prevent flow-related defects in the long-range alignment. Wire leads were attached to the ITO electrodes for electric control of the cells. When necessary, spontaneously occurring residual defects were "erased" by applying an electric field across the cell, so that large-area purely homeotropic regions of the cell could be used for optical sculpturing of desired defect patterns.

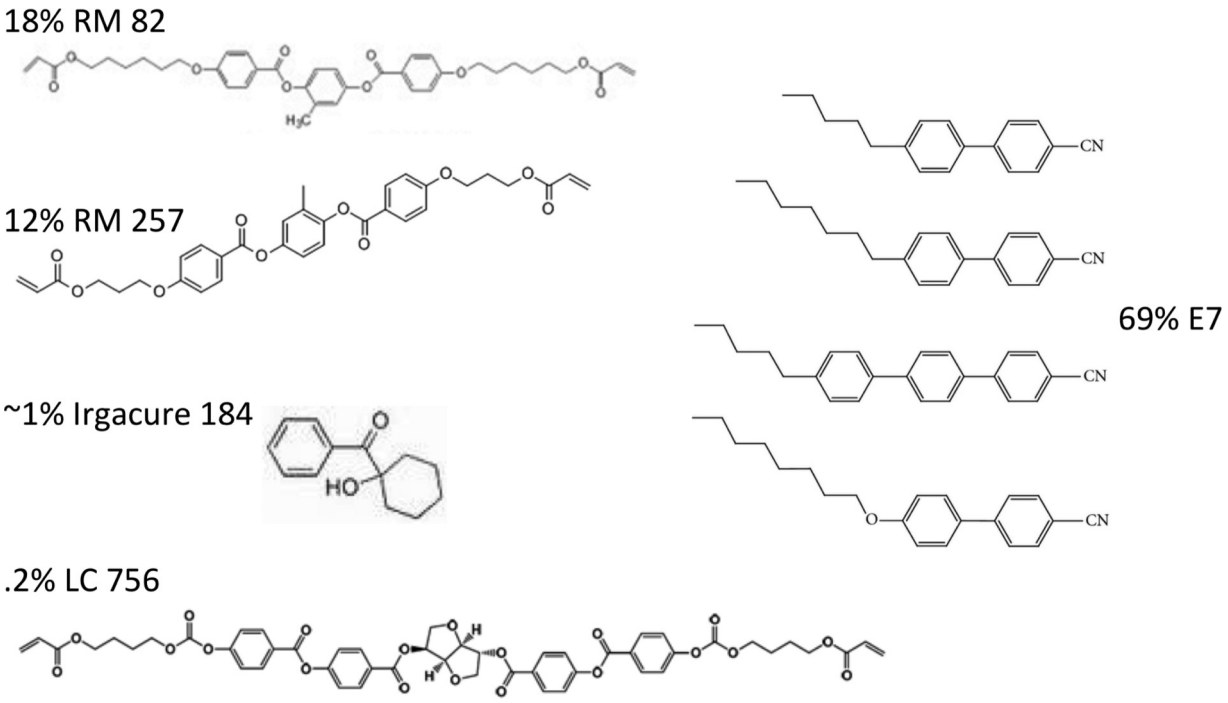

FIG. 1. Chemical composition of the partially polymerizable cholesteric mixture used: 30% diacrylate reactive mesogens RM 82 and RM 257 (top left) that can cross-link to form the polymer network, 69% nonreactive nematic mixture E7 (right), and 1% UV activated radical initiator Irgacure 184 (middle left). 99.8% of the above mixture is further mixed with 0.2% chiral diacrylate mesogen LC 756 to obtain a cholesteric LC of $p = 9\ \mu$m.

Patterns of torons and fingers were first defined using a LABVIEW-based software written by us and then drawn using the laser scanning system described below. The LC cells were then polymerized under relatively weak UV exposure (by means of a setup with a 20 W mercury bulb obtained from Cinch) to avoid thermal-gradient-induced perturbations of the optically generated LC textures with torons and fingers. For comparison, we will also discuss the morphology and structure of thin cholesteric films obtained under polymerization conditions very different from the above-described optimized conditions, in particular when using a high-intensity ~200 W UV illumination system (PCU-1, obtained from Specialty Coatings Systems, Inc.). In a typical experimental procedure for obtaining multilayer films, one of the glass substrates (typically the one farther from the UV lamp in the illumination geometry) is removed to expose the polymerized cholesteric thin film. A new wedge cell is then constructed from this substrate already containing a polymerized cholesteric film and a polyimide-SE1211-coated ITO glass plate. The 7- and 10 μm spacers in UV glue are placed directly on top of the first layer's spacers, respectively, so that the thickness d gradient directions in the two films coincide. This ensures that the regions of equal d/p overlap in the polymerized and new LC layers, thus allowing us to explore how optical generation and templating effects depend on d/p. This new cell is then infiltrated with the unpolymerized mixture to produce a second layer in which defects can be drawn and/or spontaneously form depending on the thickness of the cell and d/p. The second UV exposure is typically performed with the first polymerized layer closer to the UV source, so that the new layer can strongly adhere to the already polymerized LC film and not to the new polyimide-coated glass substrate. The removal of substrates from the partially polymerized layer does not cause noticeable damage to the partially polymerized film. The procedure of layer-by-layer polymerization of structured cholesteric films with torons and fingers can be repeated multiple times, although it soon becomes more and more technically challenging in terms of a precise control of d/p and adhesion of the polymerized cholesteric layers.

Elongated convex pentagonal and octagonal nanoprisms with length $\times$ width dimensions of 800 nm $\times$ 150 nm and 65 nm $\times$ 25 nm, respectively (to which we also refer to as gold nanorods because of their overall rodlike shapes) were obtained as ethanol-based dispersions from Nanopartz, Inc. These nanoparticles were then redispersed from ethanol to the used LC host before polymerization by means of first mixing the ethanol dispersion of nanoprisms with the LC and then evaporating ethanol. Vigorous sonication of the dispersion by means of a tip sonicator (Branson Sonfier 250, obtained from Branson Ultrasonics, Inc.) was used to break apart occasional nanoparticle aggregates.

B. Laser generation and imaging setups

Torons and fingers were generated with a laser scanning system that has been described in detail elsewhere [13,14]. Briefly, a continuous-wave ytterbium-doped collimated laser was steered by a pair of galvano mirrors powered by a digital-analog converter (NI PCI-MIO-16E-4, from National Instruments) and controlled by homemade LABVIEW-based software. The laser beam was then directed into a BX-51 upright Olympus microscope using a two-lens telescope (Fig. 2). Polarizing optical microscopy (POM) and optical manipulation were performed simultaneously while using

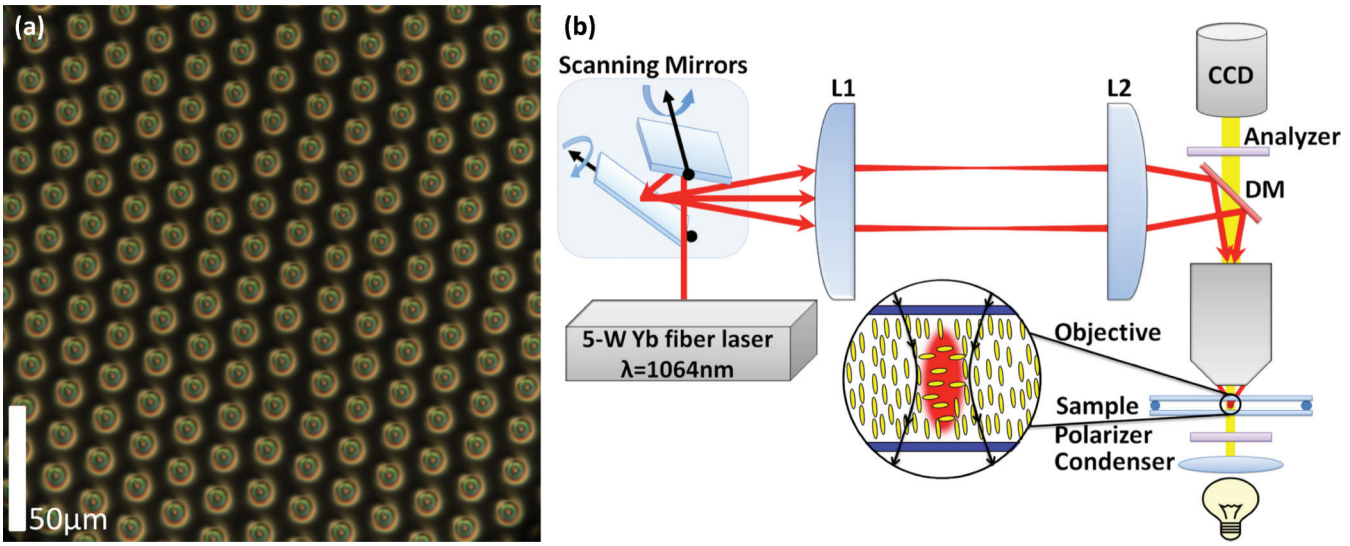

FIG. 2. (Color online) Optical generation of torons. (a) Hexagonal array of torons drawn in a thin cholesteric cell using a scanning laser system. (b) Schematic of the scanning laser generation system built around a 5 W Yb laser and galvano mirrors used to precisely position a focused laser beam in predetermined locations within the cell; this setup allows for the generation of periodic and arbitrary patterns of torons and fingers in desired locations in the LC cell. The crossed polarizer and analyzer in (a) and in all POM textures in this article are parallel to the image edges. DM is a dichroic mirror, L1 and L2 are lenses, and CCD is a charge-coupled device.

objectives with magnifications of 10×, 20×, 50×, and 100× and numerical apertures (NAs) ranging from 0.1 to 1.4.

Three-dimensional director structures in cholesteric films were probed using the noninvasive, nonlinear optical imaging technique dubbed three-photon excitation fluorescence polarizing microscopy (3PEF-PM) [41]. Biphenyl-containing LC molecules, such as the chemical compounds comprising the commercial mixture E7 (Fig. 1), have absorption and fluorescence transition dipoles along their long axis and a peak of single-photon absorption around 290 nm while fluorescing in a spectral range around 400 nm [41]. We excite them via a three-photon absorption process that gives origin to a strong $\propto \cos^6\theta$ orientational dependence of the 3PEF-PM signal intensity and inherent axial resolution in imaging of the director field $\mathbf{n}(\mathbf{r})$. The source of the 870-nm pulsed excitation is a Ti:sapphire oscillator (Coherent Chameleon Ultra-II, (680–1080)-nm excitation range, 140-fs pulse width, 80-MHz repetition rate). Laser polarization is controlled using a Glan-Thompson polarizer and half-wave waveplate. For imaging purposes, a low-power laser beam is focused with a 100× oil immersion objective (NA equal to 1.4). The focal point of the focused beam is positioned and scanned in three dimensions within the sample using a scanning head consisting of two galvano mirrors (for lateral scanning) and a stepper motor (for vertical positioning). The signal is detected with a photomultiplier tube after a 417-nm bandpass filter with 60-nm bandwidth and then used to reconstruct three-dimensional images by means of computer software.

C. Computer simulations

The equilibrium director structures of axially symmetric torons and translationally invariant fingers in single-layer cholesteric films were obtained by means of numerical minimization of elastic free energy using the director relaxation method, as described in detail elsewhere [10,14], and then used for modeling of multilayer structures studied in the present work. The model $\mathbf{n}(\mathbf{r})$ configurations in the multilayer cholesteric films were created by concatenating two single-layer director structures via superposition of $\mathbf{n}(\mathbf{r})$. The computer-simulated POM textures were then obtained for these model multilayer $\mathbf{n}(\mathbf{r})$ configurations using a Jones-matrix approach implemented in MATHEMATICA and using the experimental material and cell parameters, such as optical anisotropy, equilibrium cholesteric pitch, and cell thickness.

The initial minimum-energy $\mathbf{n}(\mathbf{r})$ configurations in the vertical cross sections of torons and fingers were represented in the form of arrays of azimuthal and polar angles, having dimensions of $99 \times 99 \times 36$ for the double-layer structures and $35 \times 35 \times 18$ and $99 \times 99 \times 18$ for the individual torons and fingers, respectively. To utilize the Jones-matrix method, we split the cell into a stack of 18 or 36 thin sublayers while assuming that the orientation of $\mathbf{n}(\mathbf{r})$ is constant across the thickness of one of these sublayers. The corresponding coordinate-dependent Jones matrices had an optical axis defined by the orientation of $\mathbf{n}(\mathbf{r})$ and the phase retardation defined by the optical anisotropy of the LC and polar angle of the director. The resulting POM texture was obtained as a result of successive multiplication of Jones matrices corresponding to a polarizer, a series of thin LC slabs each equivalent to a phase retardation plate with spatially varying optical axis and retardation, and an analyzer. A two-dimensional POM image was then obtained by performing such a Jones-matrix calculation for each pixel and then composing a two-dimensional texture with coordinate-dependent POM intensity analogous to the experimental images. To properly account for the achromatic nature of our experimental POM observations, we calculated these textures separately for three different wavelengths spanning the entire visible spectrum (475, 510, and 650 nm) and then

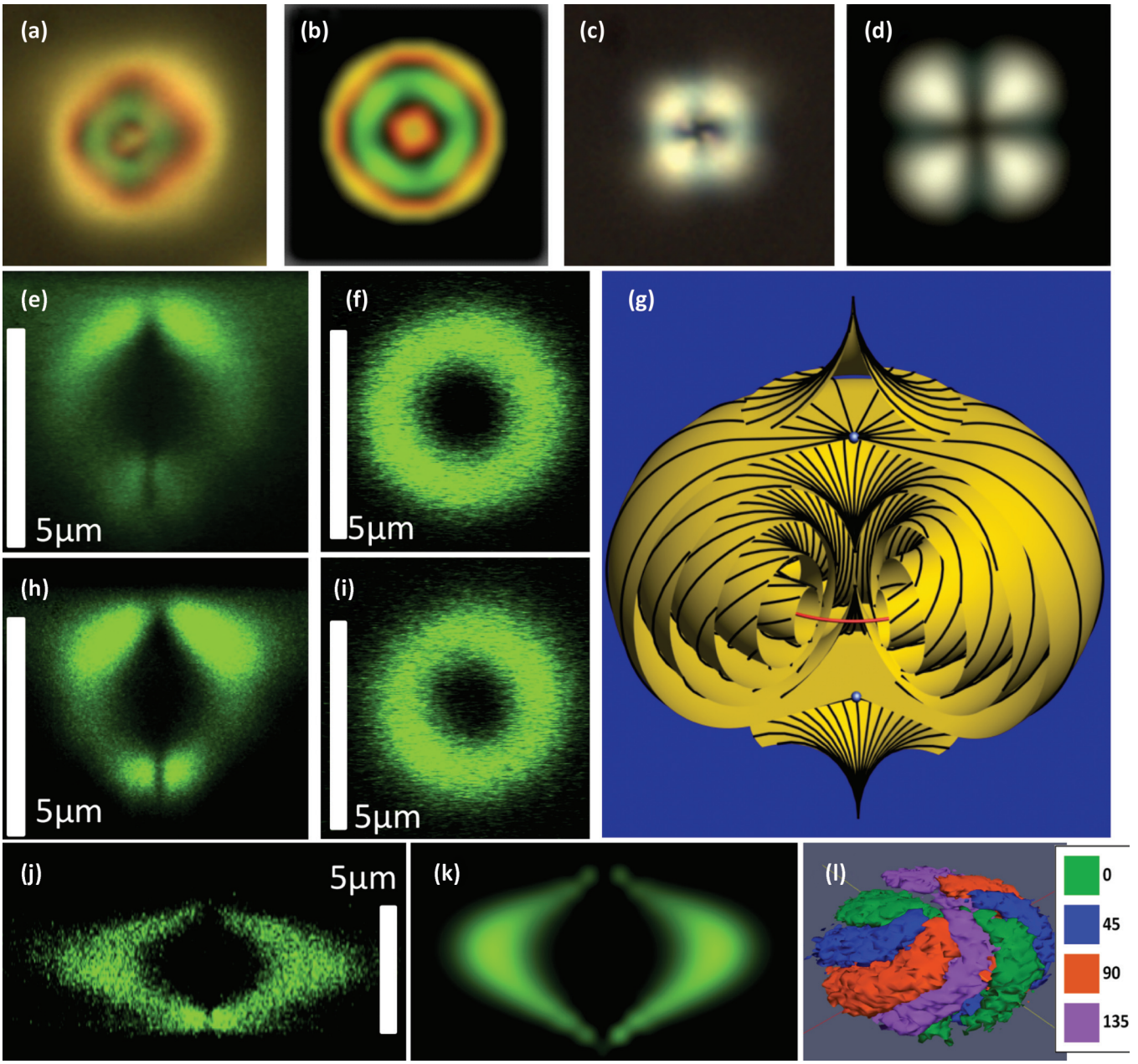

FIG. 3. (Color online) Imaging and computer simulations of polymerized and unpolymerized torons. (a) Experimental POM image of a polymerized toron. (b) Computer-simulated POM image of a toron obtained using experimental parameters. (c) A POM image of a polymerized toron after washing away the unpolymerized LC with IPA. (d) Computer-simulated POM image of a toron with reduced birefringence produced by adjusting the residual birefringence value to match the appearance of the experimental POM image. (e)–(k) In-plane xy [(f) and (i)] and vertical xz [(e), (h), (j), and (k)] 3PEF-PM cross-sectional images of the toron obtained before [(e) and (f)] and after [(h) and (i)] polymerization show that the three-dimensional $\mathbf{n}(\mathbf{r})$ structure of the toron is unchanged during the polymerization process. (g) Schematic of the $\mathbf{n}(\mathbf{r})$ structure of a toron [10]. (j) A 3PEF-PM vertical cross section of a polymerized toron after the unpolymerized E7 was replaced by an immersion oil shows a much more symmetric cross section (j) as compared to (e) and (h) due to the large reduction in birefringence and consequent sample lensing and scattering that typically cause imaging artifacts; this experimental image closely matches its computer-simulated counterpart shown in (k). The 3PEF-PM images shown in (e), (f), and (h)–(k) were obtained using circularly polarized excitation light. (l) Three-dimensional visualization of the toron structure obtained by combining four three-dimensional images of this polymerized toron (in which E7 was replaced by an immersion oil), where high-intensity regions of fluorescence textures are depicted by colors that depend on the orientation of linear polarization of the excitation light at 0, 45°, 90°, and 135° with respect to the x direction marked by the red line running from bottom-left to top right.

superimposed them to obtain the white-light simulated POM image. Computer-simulated vertical 3PEF-PM cross sections were obtained for the same equilibrium director structures by first finding the coordinate-dependent angles θ between $\mathbf{n}(\mathbf{r})$ and the linear polarization of the probing laser light and then plotting the normalized signal intensity as $I_{\text{3PEF-PM}} \propto \cos^6\theta$

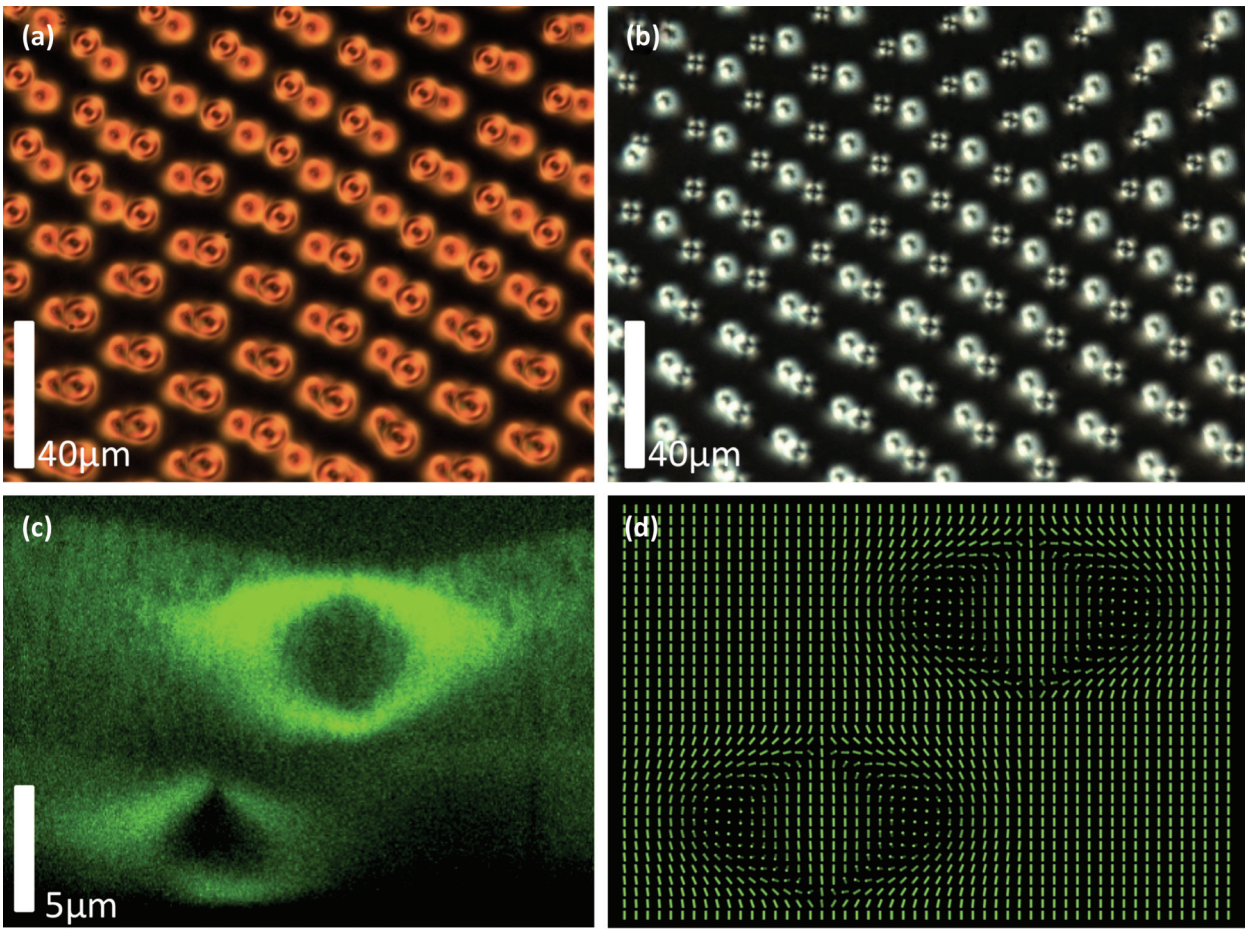

FIG. 4. (Color online) Two-layer arrays of optically generated torons. (a) A POM image of polymerized torons in a two-layer cholesteric film; to obtain it, an optically generated hexagonal array of torons in the first layer was used as a template for localization of torons in the second layer and was then followed by polymerization of the second layer. (b) A similar two-layer array of torons imaged after the E7 was washed out by solvent and the nanoporous cholesteric film was infiltrated with an immersion oil. (c) Vertical cross section of the sample with two torons in different cholesteric layers obtained by means of 3PEF-PM imaging with circularly polarized excitation light. (d) Numerical model of the director field showing how the use of a first layer with a toron array causes an offset of optically generated torons in the second layer before its polymerization; the spatial variations of the director field are shown using cylinders.

[41]. All experimental and computer-simulated images of $\mathbf{n}(\mathbf{r})$ structures in single and multilayer cholesteric films closely match each other and strongly support the interpretation of experimental findings that we describe below.

III. RESULTS

A. Preparation of single-layer cholesteric cells

The generation of fingers and torons in nonreactive confined cholesteric LCs has been demonstrated in our previous publications [10–14] and implemented using both Gaussian and vortex laser beams. In partially reactive cholesteric systems studied in this work, the generation of torons occurs through the same procedure of focusing a Gaussian 1064 nm beam in the desired location for around 0.1 s (Fig. 2). The partially polymerizable mixture used (Fig. 1) was chosen due to its positive dielectric anisotropy, room-temperature nematic state, and strong homeotropic surface anchoring that can be set on confining substrates by use of polyimides. The ground-state configuration of the LC director is sensitive to the ratio of cell thickness d to pitch p. A (7–10) μm wedge cell having width of 1–2 cm typically gives a uniformly unwound $2 \times 2\,\mathrm{mm}^2$ homeotropic region with $d/p = 0.7$–1, in which one can optically generate the toron and finger structures [10–14]. The thicker part of this wedge cell ($d/p > 1$) contains spontaneously occurring fingers and other localized structures, while the thinner part ($d/p < 0.6$) contains a fully unwound homeotropic state in which optically generated localized structures are unstable and relax back to the uniform configuration with vertical director. Although the wedge geometry of the cells is unnecessary and similar results can be obtained for flat cells of constant thickness and well-controlled values of d/p, wedge cells allow for a facile exploration of how the studied optical generation and templating effects depend on d/p.

B. Partial polymerization of the structured cholesteric films

One of the main challenges in photopolymerization of cholesteric configurations is to preserve the director field of the LC during the polymerization process. Because of the absorption of UV light as it traverses the LC medium, the

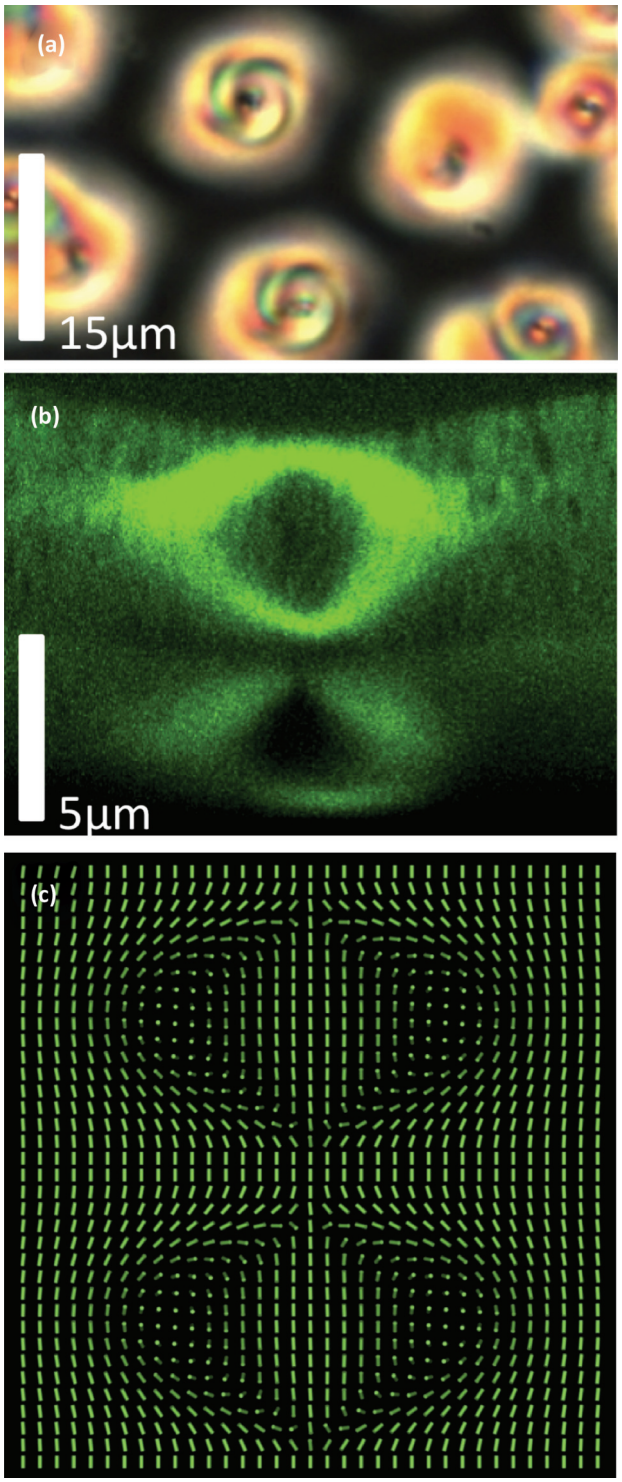

FIG. 5. (Color online) Coaxial arrangement of torons in a two-layer polymerized cholesteric film. (a) A POM image of the two-layer structure with a toron located directly on top of another toron in the templating cholesteric layer. (b) Vertical cross section of a two-layer film having torons in the second layer positioned directly on top of torons of the first layer obtained using 3PEF-PM with circularly polarized excitation light. (c) A numerical model of the director field shows that the first cholesteric layer with a toron can also cause a localization of an optically generated toron in the second layer before its polymerization that is coaxial with the toron in the polymerized templating layer.

polymerization of a partially polymerizable mixture occurs faster near the UV source and typically causes the nonreactive components of the mixture to concentrate farther away from the UV source. If the chiral dopant is fully reactive, this process causes the cholesteric pitch gradients with the shortest pitch being at the cell substrate closer to the UV illumination source. If the chiral dopant is nonreactive, however, this process causes the pitch to decrease in the polymerized parts, thus resulting in pitch gradients analogs to pitch-gradient cholesteric polymers formed by polymerizing chiral and nematic monomers with unequal reactivity [42]. The UV exposure can also cause significant amounts of heating and lead to potential phase changes, gradients of pitch due to the temperature dependence of helical twisting power of the used chiral dopants, or even gradients of the scalar order parameter. Heating and decreasing the pitch can lead to the development of the translationally invariant configuration (TIC) from the initially homeotropic regions [12–14], as well as tilting and merging of torons with the TIC in the cell midplane. Although the director configurations of polymerized cholesteric films in this case significantly differ from the ones in the fluid LC samples and would not be stable in nonpolymerized systems, these TIC-embedded toron structures have not been achieved before in nonpolymerizable systems and show how this polymerizable system can potentially be used for the exploration of nonequilibrium configurations of polymerized confined cholesteric LCs.

We have optimized the polymerization process by selecting a reactive chiral dopant and using relatively low light exposure for cross-linking of the cholesteric films so that the three-dimensional structures of torons and fingers can be "frozen" by polymerization in a solid film without altering their initial director configuration (Fig. 3). We verify this by obtaining 3PEF-PM cross-sectional images before [Figs. 3(e) and 3(f)] and after [Figs. 3(h) and 3(i)] the polymerization. The unpolymerized E7 in this partially cross-linked system can be partially removed by addition of isopropanol. This allows for the reduction of the medium's effective birefringence by up to approximately one order of magnitude without disrupting the director structure of this partially polymerized system (Figs. 3 and 4). The residual birefringence is primarily due to the cross-linked part of the partially polymerized cholesteric film and small amounts of unwashed E7 entrapped within the partially polymerized film in the LC state.

The asymmetry of the vertical cross sections shown in Figs. 3(e) and 3(h) with respect to the cell midplane is due to the absorption, scattering, and defocusing of the 3PEF-PM laser excitation light as it traverses farther away from the objective in the LC medium of high optical birefringence. Because of the reduced birefringence, the 3PEF-PM vertical cross sections of samples with E7 partially replaced by an isotropic solvent become significantly less asymmetric with respect to the cell midplane (since the scattering- and defocusing-related artifacts are partially mitigated) and closely match the corresponding computer-simulated 3PEF-PM images [Figs. 3(j) and 3(k)]. This artifact-free three-dimensional 3PEF-PM imaging using four different linear polarization states of excitation light also allows for visualization of topology of the toron structure in a ParaView presentation [Fig. 3(l)] resembling the so-called Pontryagin-Thom construction [9].

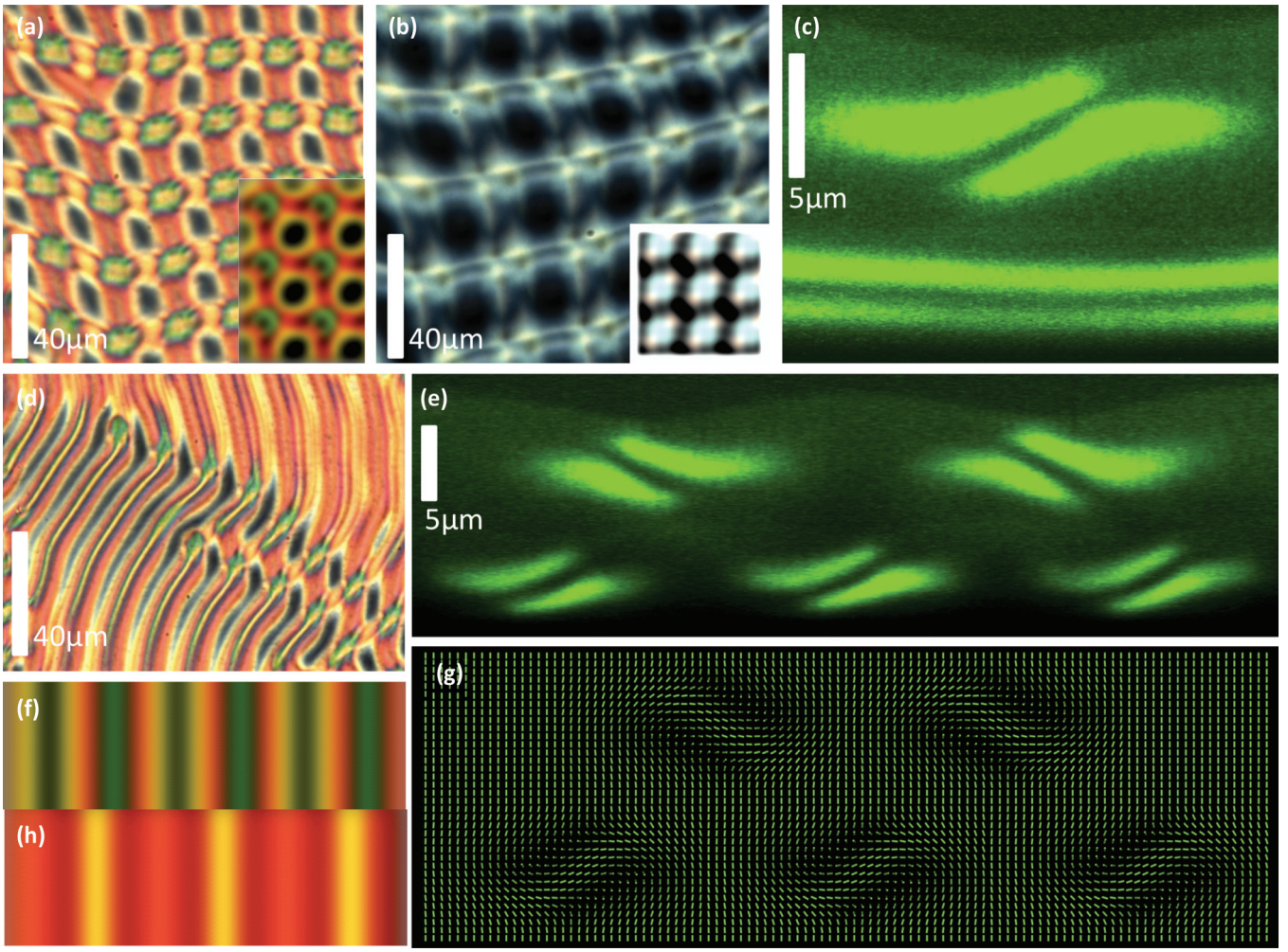

FIG. 6. (Color online) Two-layer polymerized structures with cholesteric fingers. (a) and (b) Cholesteric fingers that nucleate in a second fluid cholesteric layer (before its polymerization) on top of a polymerized cholesteric layer with fingers typically spontaneously align perpendicular to the fingers in the first templating layer, as observed in POM images (a) before and (b) after replacing E7 of the partially polymerized LC with an immersion oil. The corresponding computer-simulated POM textures are shown as bottom-right insets of (a) and (b). The values of cell thickness and effective optical anisotropy used to obtain these computer-simulated images correspond to experimental values (e.g., $\Delta n_{\text{eff}} \approx 0.03$ for the film with the E7 replaced by immersion oil, almost an order of magnitude lower than the optical anisotropy of $\Delta n = 0.22$ of E7) at which the experimental and computer-simulated images closely match each other, as shown in (b). (c) A vertical 3PEF-PM cross section of the sample along a finger in the bottom templating layer and corresponding to the POM texture shown in (b); the linear polarization direction of laser excitation light in 3PEF-PM is perpendicular to the image. (d) A POM image showing that the fingers in the second layer can also align parallel to the fingers in a templating polymerized layer. (e) Vertical 3PEF-PM cross section reveals that the helical axes of twist in fingers that align parallel to each other in the two layers always tilt in opposite directions with respect to the cell normal; the linear polarization direction of laser excitation light in 3PEF-PM is perpendicular to the image. (f) and (h) computer-simulated POM textures for parallel fingers obtained for two different shifts of fingers in the two layers on top of each other. As the parallel fingers in the top layer slightly shift with respect to the bottom layer, they produce dramatically different POM textures, as seen in the various regions of (d) and simulated for lateral shifts (f) $\approx p/3$ and (h) $\approx p/2$. (g) Numerical model of the director field in the two-layer cholesteric film corresponding to the 3PEF-PM cross section shown in (e); the spatial variations of the director field are shown using cylinders.

C. Preparation of multilayer polymerized structures

To obtain three-dimensional patterns of torons and fingers, we first fabricate two-layer cells with collocated regions of d/p of interest (Fig. 4). A single-layer cell with a partially polymerized cholesteric film (obtained as described above) is split apart so that the cholesteric film remains attached to one of the two substrates. This substrate with the partially polymerized thin film is then used to form a new two-layer cholesteric cell. The process of polymerizing and opening of a single-layer cell produces slight thickness variations in the polymerized film [visible in vertical 3PEF-PM cross sections such as the one in Fig. 4(c)] due to the presence of topological defects and spatially varying $\mathbf{n}(\mathbf{r})$. This then results in the corresponding slight thickness variations of the new cholesteric layer, which is complementary to the thickness profile of the polymerized film. The ensuing interaction of cholesteric structures then results in templating of certain

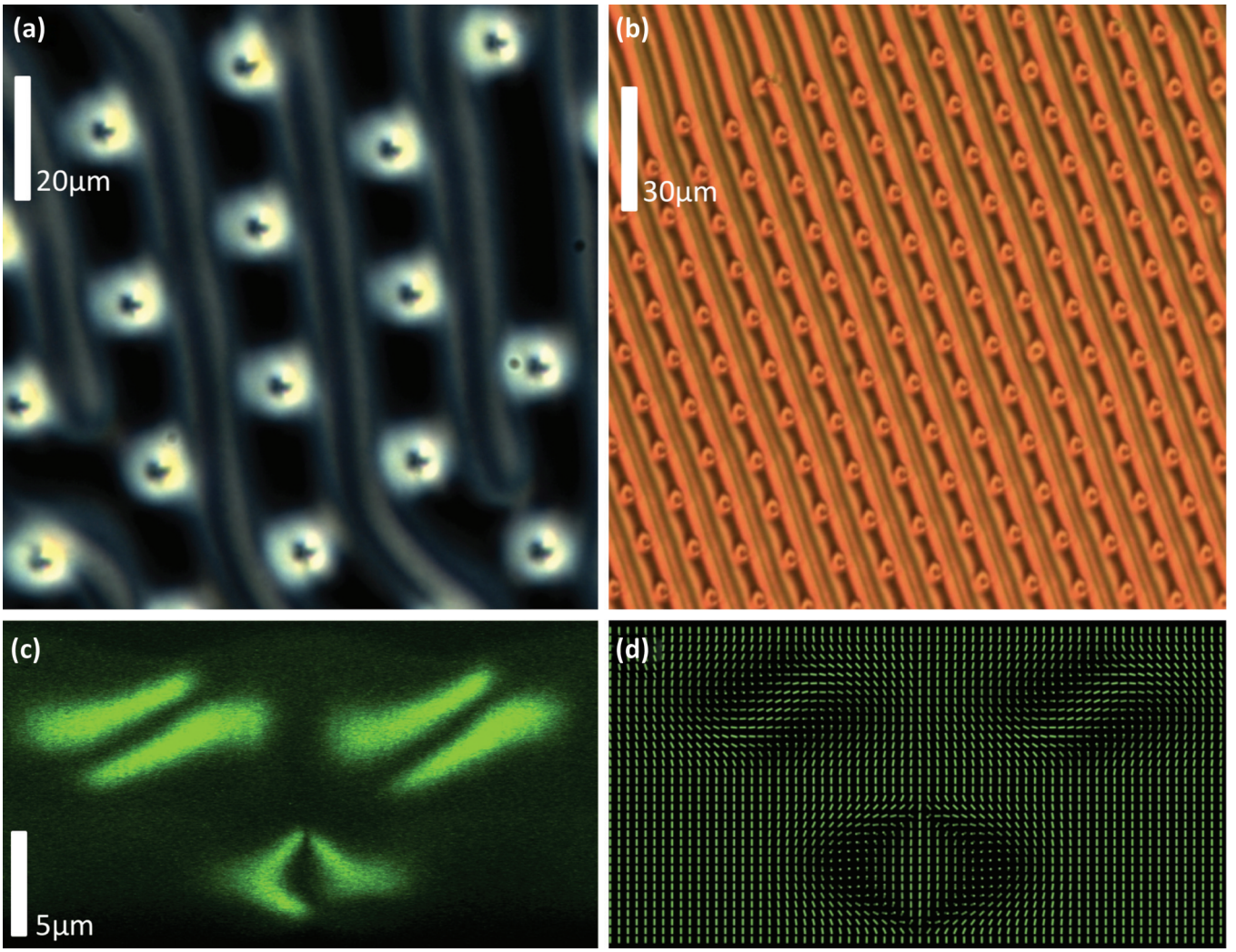

FIG. 7. (Color online) Hybrid two-layer structure with torons in the templating layer and fingers in the second layer. (a) A POM image of the film after washing out E7 and infiltration of the nanoporous structure with immersion oil. (b) A POM image for a similar film with E7 present in it. (c) Experimental 3PEF-PM vertical cross section of the film shown in (a) obtained along a line perpendicular to the fingers. (d) Numerical model of the director field in a two-layer film corresponding to the image shown in (c). Note that the location and orientation of fingers templated in the second cholesteric layer are predetermined by the optically generated hexagonal lattice of torons in the polymerized templating layer.

well-defined director configurations in the new LC layer, which are highly dependent on d/p and the particular localized structures formed within the polymerized and unpolymerized LC layers in contact. When we use laser tweezers to optically "draw" an array of torons in the fluid layer initially laterally offset from the polymerized layer's toron array, we observe little or no lateral movement of defects and structural changes in the newly generated array of torons in the fluid LC part of the cell (Fig. 4). However, if we draw the new torons directly on top of the torons of the templating polymerized layer, they shift off (so that the toron arrays in the two layers are eventually offset with respect to each other), although even in this case there is a small window of d/p values for which coaxial alignment of torons in the two layers is possible (Fig. 5).

Interactions between director structures of polymerized and unpolymerized layers are also present in cholesteric films containing either optically drawn and spontaneously occurring configurations of fingers (Figs. 6–8). Multiple types of finger-finger and finger-toron interactions can occur depending on the d/p ratio. When we optically draw torons on top of fingers in the polymerized templating layer, we observe a strong attraction of these torons to well-defined equilibrium lateral positions with respect to fingers; this interaction transforms the initially periodic lattice of laser-drawn torons to a pattern templated by the location of fingers in the polymerized layer [Figs. 8(d) and 8(e)]. When the unpolymerized layer with d/p ratio between 0.9 and 1.0 is somewhat thicker than the polymerized one, fingers in the unpolymerized layer can spontaneously grow and follow the patterning set by cholesteric structures in a polymerized layer. If the polymerized layer contains fingers, the new fingers grow predominantly perpendicular [Figs. 6(a) and 6(b)] and sometimes parallel to the polymerized-layer fingers [Fig. 6(d)], but not at intermediate angles between 0 and $\pi/2$. When the

fingers grow parallel to the polymerized fingers, the helical axes defining the directions of twist in fingers in the two layers are always tilted in opposite directions [Figs. 6(e) and 6(g)]; they also predominantly grow out of phase with the polymerized-layer fingers [as seen in the upper right of Fig. 6(e)) and confirmed in the corresponding computer simulations of POM textures shown in Figs. 6(f) and 6(g)], i.e., on top of homeotropic regions interspacing the fingers of the templating polymerized layer. When fingers are spontaneously growing on top of a laser-drawn polymerized-layer periodic array of torons, they tend to pass between the toron rows along one of the hexagonal lattice axes of the underlying array (Fig. 7). However, within a certain well-defined range of d/p between 0.9 and 1.0 in the unpolymerized layer, the fingers can also grow on top of the rows of torons [Figs. 8(a)–8(c)], with the finger axis being only slightly misaligned with respect to the hexagonal lattice axis [Fig. 8(a)].

The 3PEF-PM vertical cross sections of polymerized cholesteric films with torons and fingers show a slight bulge in the film that correlates with the spatial locations of these structures, which indicates that observed templating interactions may be caused by (a) the corresponding variations of effective thickness of unpolymerized films and (b) elastic interactions that arise from slight variations of the LC easy axis at the interface with the polymerized layer. Our findings demonstrate that interactions between cholesteric structures of two-layer unpolymerized and partially polymerized LC films can result in templating of spontaneously occurring and optically generated structures that can be controlled via varying d/p ratios of the two films in contact. By varying d/p, one can obtain arrays of torons and fingers that are collocated, displaced, and differently oriented with respect to each other in different layers of multilayer partially polymerized cholesteric films. Moreover, by controlling the kinetics of the polymerization process itself (Fig. 9), it is also possible to obtain polymerized nonequilibrium director patterns with defects that would be unstable without using such procedures.

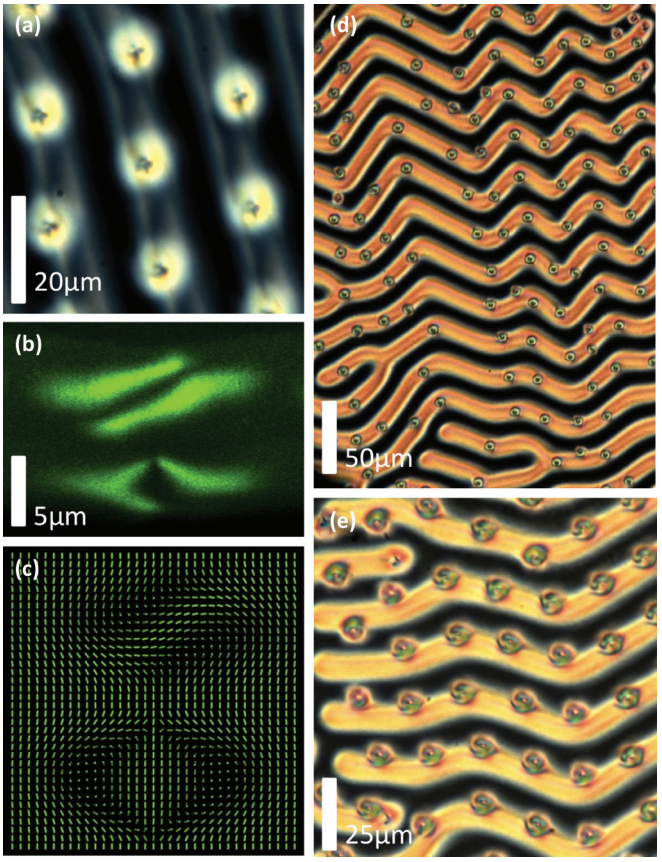

FIG. 8. (Color online) Vertically collocated toron-finger configurations. (a) A POM image of a cholesteric two-layer film with fingers positioned on top of a row of torons and with E7 replaced by immersion oil. (b) The 3PEF-PM vertical cross section corresponding to (a) and obtained along a line perpendicular to the fingers and using excitation light with linear polarization perpendicular to the fingers. (c) Numerical model of the director field in the two-layer film corresponding to the vertical cross section shown in (b). (d) and (e) POM images of a two-layer film with optically generated torons in a nonpolymerized layer that interact with the cholesteric fingers in a polymerized templating layer.

D. Polymerization of structures with metal nanoparticles entrapped by defects

In unpolymerized fluid LCs, topological defects spontaneously attract, spatially entrap, and align nanoparticles so that the nanoparticles can displace energetically costly regions of defect cores with reduced order parameter and the surrounding LC with strong elastic distortions while minimizing the total free energy [Fig. 10(a)] [31]. Dark-field imaging allows particles of size ~10 nm and larger to be detected (based on their characteristic scattering of light) and correlated with the location of singular topological defects that also scatter light [Fig. 10(a)]. As an example, we demonstrate in Fig. 10(a)) the observation of a 150 nm × 800 nm gold nanorod being attracted to the hyperbolic point defect of a toron structure [Figs. 10(a) and 10(b)]. Since the average size of the isotropic core of a LC defect is typically within 10–100 nm [16,31] in nonpolymerized systems, particles can be spectroscopically and microscopically observed (despite some amount of orientational and positional averaging associated with the defect-constrained Brownian motion). Polarized dark-field imaging reveals that the nanorod orients roughly along the cell normal, as depicted in the schematic of Fig. 10(e). Similar oriented entrapment was also observed for the smaller studied gold nanorods with dimensions 65 nm × 25 nm, indicating that the demonstrated spatial patterning of anisotropic nanoparticles in defects and defect arrays can be extended to nanoparticles with a broad range of nanoscale sizes.

Photopolymerization allows for the mitigation of the residual Brownian motion associated with a trapped nanorod and provides a stable position and orientation of the nanoparticle within the bulk of a sample, as needed for spectroscopic studies and microscopic observation [Figs. 10(c) and 10(d)]. Furthermore, properties of the matrix surrounding the nanoparticle entrapped by the defect can be controlled by varying the composition of unpolymerized parts of this partially polymerized film without altering the nanoparticle's localization and orientation with respect to defects and the far-field director. For example, the infiltration with isopropanol or immersion oil (which displaces a large fraction of the

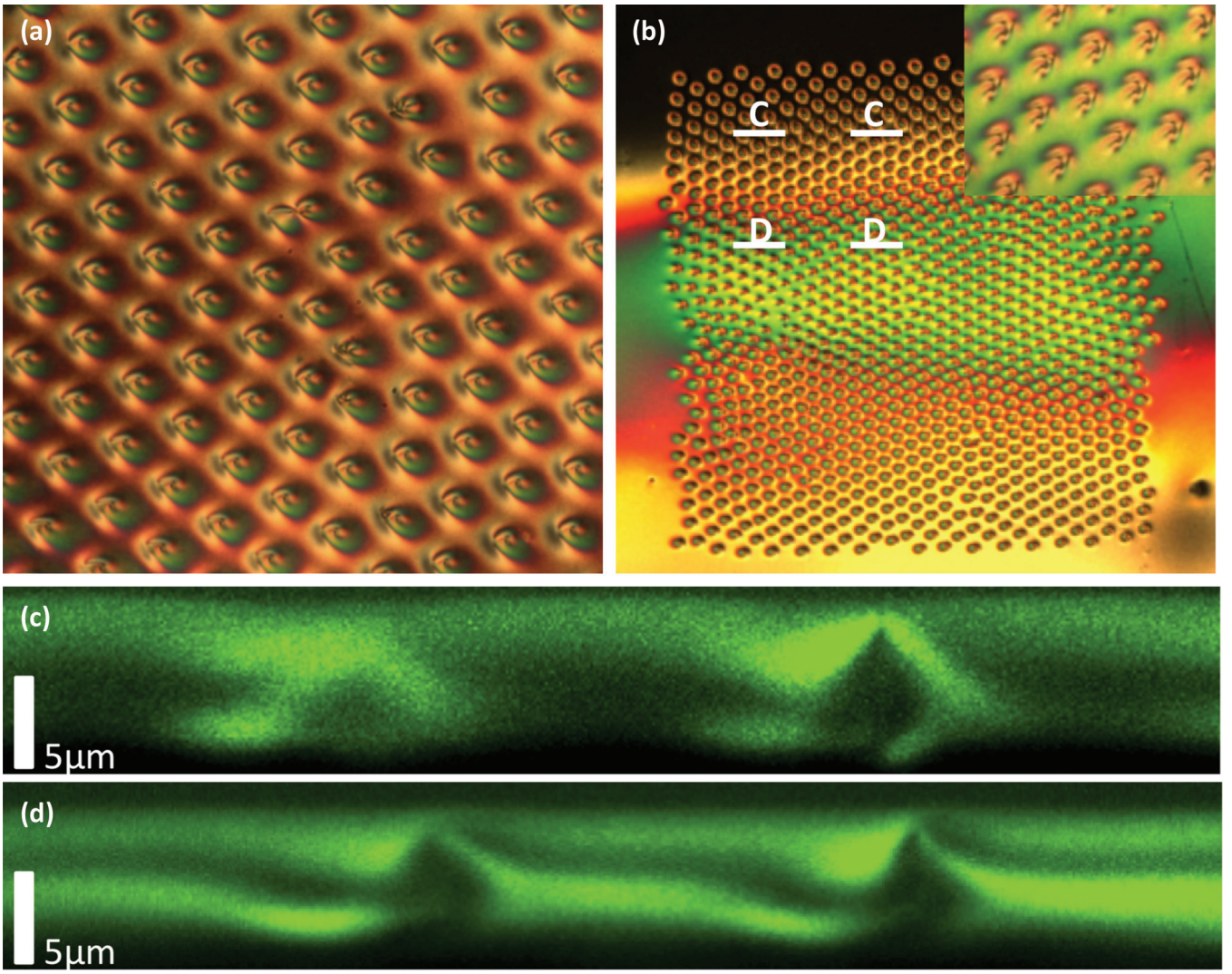

FIG. 9. (Color online) Tilting of torons and generation of TIC caused by different polymerization procedures: (a) because of polymerization-induced gradients of chiral dopant concentration in a partially polymerizable cholesteric film with nonreactive chiral additive CB15 used instead of LC 756 and (b) due to thermal effects associated with high-intensity UV exposure used for cross-linking; the details of the POM texture are shown in the inset. (c) and (d) The 3PEF-PM vertical cross sections of "tilted torons" from the regions of the POM image shown in (b) and marked correspondingly as *C*-*C* and *D*-*D* cross sections on the POM image; vertical cross sectionswere imaged with linearly polarized excitation light with polarization direction perpendicular to the page.

unpolymerized E7 component of the film) does not disturb the nanoparticle's orientation and relative position but allows us to significantly reduce the effective optical anisotropy of the matrix surrounding the nanoparticle (Fig. 10).

IV. DISCUSSION

The interactions between polymerized and unpolymerized cholesteric layers in contact with each other reveal out-of-plane attractions and repulsions between localized cholesteric structures of torons and fingers that cannot be observed in conventional single-layer LC cells. These effects can potentially be used for templated layer-by-layer structural self-assembly leading to large-scale production of well-ordered films with periodic three-dimensional patterns of LC defects. A robust control of these interactions requires precise control of the d/p ratio, which can be achieved for flat LC cells with parallel substrates and well-defined cell gaps. When undesirable, these interactions can be mitigated or eliminated by using a fully polymerizable LC mixture and recoating the polymerized matrix with polyimide after the addition of each new layer. The addition of new cholesteric layers can in principle be carried out *ad infinitum*, however, the practical realization of films with large numbers of layers is hindered by the difficulty of proper splitting of multilayer cells, rather tenuous adhesion of new layers to the templating layers, and other technical factors. Under proper clean room conditions with an automated placement of spacer particles dispersed within UV glue to set uniform cell gap, this process could be readily used to create three-dimensional inch-scale defect arrays with and without nanoparticles decorating the LC singularities.

Localization and orientation of anisotropic nanoparticles in the energetically costly defect cores of topological structures in cholesteric LCs can be extended to a wide range

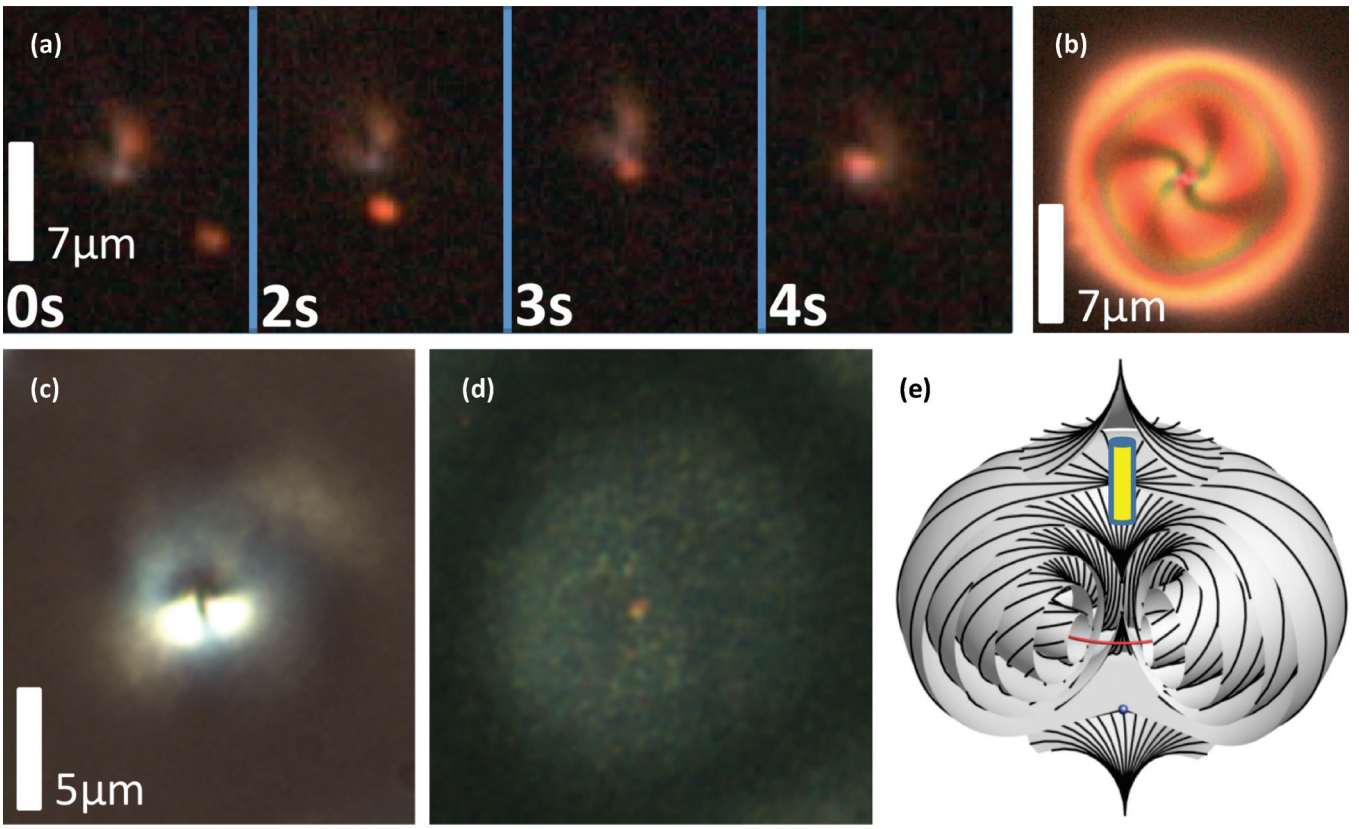

FIG. 10. (Color online) Spatial localization of gold nanoparticles in hyperbolic point defects within a toron. (a) Dark-field microscopy time sequence showing an elongated pentagonal gold nanoprism (having a length of 800 nm and transverse size of about 150 nm) being spontaneously attracted to the point defect of a toron structure; the elapsed time is marked on the images. (b) Colocated POM image of the same toron as shown in (a) having the gold nanoparticle entrapped by the hyperbolic point defect. (c) and (d) 25 nm $\times$ 65 nm rodlike nanoparticle in a polymerized cholesteric film containing a toron as seen in (c) bright-field POM and (d) dark-field images and schematically depicted in (e).

of length scales and nanoparticle material compositions, including metallic, semiconducting, and dielectric particles. Since the localized cholesteric structures can be generated and spatially translated by the optical trap, well-controlled assemblies of one or a few nanoparticles can be generated by actively entrapping specific nanoparticles one wants to collect for a detailed analysis (e.g., for probing nanophotonic interactions between individual and small groups of plasmonic nanoparticles and quantum dots). We have previously demonstrated such entrapment of single and multiple nanoparticles using the hyperbolic hedgehog point defects induced by microspheres with homeotropic boundary conditions [31]. The present work demonstrates the feasibility of similar entrapment in LCs even without the use of microspheres and in the form of three-dimensional architectures defined by defects in multilayer, polymerizable cholesteric films. This type of nanoparticle patterning in defects and their arrays may provide means of exploring nanoscale energy conversion in single and small groups of quantum dots, rods, and disks, as well as plasmonic enhancement of various effects such as multiple exciton generation at precisely controlled nanoscale length scales. Partial polymerization of the LC in the studied multilayer cholesteric films allows for "locking in" of desired architectures of self-assembled nanoparticles. The porous nature of such partially polymerized films allows for replacing a major fraction out of the 70% of unpolymerized E7 by various other LCs or isotropic solvents, thus controlling optical anisotropy, effective dielectric constants, and other properties of the surrounding LC matrix. This in turn may provide the means of probing how the interactions between defect-entrapped nanoparticles depend on the surrounding medium's optical and dielectric properties. Furthermore, combining periodic patterns of spatially varying LC optical axis and defect-entrapped arrays of plasmonic metal nanoparticles may be of interest for many photonic applications where new photophysical properties arise from controlling the mesoscale structure and composition of organic-inorganic composites.

The 3PEF-PM vertical cross sections show that the replacement of the E7 unpolymerized component of partially polymerized films by immersion oil causes the homeotropic regions of the film to swell more than the regions containing topological defects and various twisted structures, as we show in Figs. 4(c), 5(b), 6(c), 6(e), 7(c), and 8(b). Although the exact physical underpinnings behind such anisotropic swelling and deswelling are unknown, this effect may be potentially extended to azobenzene-containing polymerizable systems, in which surface profiles of thin films may be potentially controlled via optical illumination. The templating and anisotropic orientation-sensitive swelling effects may potentially also be extended from the flat thin-film geometry

used in the present work to that of multilayer shells, pillars, and films with grain boundaries and line defects [43–45], as well as to LC-colloidal composites containing particles with various topology and composition [46].

The use of a partially polymerized LC system ensures continuity of the director field between different layers of the multilayer films with defects. Therefore, our approach will enable both three-dimensional patterning and imaging of complex director configurations with defects, thus allowing for experimental exploration of relations between the topologies of LC director fields, defects, and surfaces of various colloidal inclusions [46]. The combination of optical generation of chirality-stabilized director structures, their photopolymerization, and then three-dimensional optical imaging of director fields with improved resolution brings about a set of experimental techniques that may allow researchers to answer a number of open questions related to the nature and properties of LC defects [23,46].

V. CONCLUSION

We have demonstrated that optical generation, spontaneous templating, and partial polymerization allow for the stabilization of cholesteric finger and toron structures and the formation of three-dimensional arrays of defects by the vertical stacking of thin cholesteric films. Three-dimensional patterning of defects allows for templating of plasmonic nanoparticles that decorate LC singularities and their arrays, laying the groundwork for potential applications in nanophotonics, plasmonics, nanoscale energy conversion, and metamaterial fabrication. The experimental arena that we have developed will provide researchers with a powerful means of studying the interplay of topology of defects and director fields in confined chiral liquid crystals that will impinge on understanding defects and topologically nontrivial fields in other condensed matter systems.

ACKNOWLEDGMENTS

This work was supported by the Division of Chemical Sciences, Geosciences, and Biosciences, Office of Basic Energy Sciences of the US Department of Energy under Contract No. DE-AC36-08GO28308 with the National Renewable Energy Laboratory (J.v.d.L. and P.J.A.) and by NSF Grant No. DMR-0847782 (J.S.E. and I.I.S.). We acknowledge discussions with Nick Abbott, Noel Clark, Angel Martinez, Bohdan Senyuk, and Tim White.

[1] T. H. Skyrme, Proc. R. Soc. London Ser. A **260**, 127 (1961).
[2] S. Muhlbauer *et al*., Science **323**, 915 (2009).
[3] S. Heinze, K. von Bergmann, M. Menzel, J. Brede, A. Kubetzka, R. Wiesendanger, G. Bihlmayer, and S. Blügel, Nat. Phys. **7**, 713 (2011).
[4] M. Uchida and A. Tonomura, Nature (London) **464**, 737 (2010).
[5] J. Verbeeck, H. Tian, and P. Schattschneider, Nature (London) **467**, 301 (2010).
[6] L. Allen, M. W. Beijersbergen, R. J. C. Spreeuw, and J. P. Woerdman, Phys. Rev. A **45**, 8185 (1992).
[7] M. R. Dennis, R. P. King, B. Jack, K. O'Holleran, and M. J. Padgett, Nat. Phys. **6**, 118 (2010).
[8] I. Chuang, R. Durrer, N. Turok, and B. Yurke, Science **251**, 1336 (1991).
[9] B. G. Chen, P. J. Ackerman, G. P. Alexander, R. D. Kamien, and I. I. Smalyukh, arXiv:1212.6688 [cond-mat.soft].
[10] I. I. Smalyukh, Y. Lansac, N. A. Clark, and R. Trivedi, Nat. Mater. **9**, 139 (2010).
[11] O. Trushkevych, P. Ackerman, W. A. Crossland, and I. I. Smalyukh, Appl. Phys. Lett. **97**, 201906 (2010).
[12] I. I. Smalyukh, D. Kaputa, A. V. Kachynski, A. N. Kuzmin, P. J. Ackerman, C. W. Twombly, T. Lee, R. P. Trivedi, and P. N. Prasad, Opt. Express **20**, 6870 (2012).
[13] P. J. Ackerman, Z. Qi, and I. I. Smalyukh, Phys. Rev. E **86**, 021703 (2012).
[14] P. J. Ackerman, Z. Qi, Y. Lin, C. Twombly, M. Laviada, Y. Lansac, and I. I. Smalyukh, Sci. Rep. **2**, 414 (2012).
[15] U. Tkalec, M. Ravnik, S. Čopar, S. Žumer, and I. Muševič, Science **333**, 62 (2011).
[16] P. M. Chaikin, and T. C. Lubensky, *Principles of Condensed Matter Physics* (Cambridge University Press, Cambridge, 2000).
[17] J. Charvolin and J. F. Sadoc, Eur. Phys. J. E **25**, 335 (2008).
[18] P. Oswald, J. Baudry, and S. Pirkl, Phys. Rep. **337**, 67 (2000).
[19] I. I. Smalyukh, B. I. Senyuk, P. Palffy-Muhoray, O. D. Lavrentovich, H. Huang, E. C. Gartland, V. H. Bodnar, T. Kosa, and B. Taheri, Phys. Rev. E **72**, 061707 (2005).
[20] J. W. Milnor, *Topology from the Differentiable Viewpoint* (The University Press of Virginia, Charlottesville, 1965).
[21] C. Phatak, A. K. Petford-Long, and O. Heinonen, Phys. Rev. Lett. **108**, 067205 (2012).
[22] R. P. Trivedi, I. I. Klevets, B. Senyuk, T. Lee, and I. I. Smalyukh, Proc. Natl. Acad. Sci. USA **109**, 4744 (2012).
[23] G. Alexander, B. Chen, E. Matsumoto, and R. Kamien, Rev. Mod. Phys. **84**, 497 (2012).
[24] I. I. Smalyukh, D. Kaputa, A. V. Kachynski, A. N. Kuzmin, and P. N. Prasad, Opt. Express **15**, 4359 (2007).
[25] J. Pérez-Juste *et al*., Coord. Chem. Rev. **249**, 1870 (2005).
[26] N. Jana, L. Gearheart, and C. Murphy, J. Phys. Chem. B **105**, 4065 (2001).
[27] A. P. Alivisatos, Science **271**, 933 (1996).
[28] X. Peng, L. Manna, W. Yang, J. Wickham, E. Scher, A. Kadavanich, and A. P. Alivisatos, Nature (London) **404**, 59 (2000).
[29] A. J. Nozik, Chem. Phys. Lett. **457**, 3 (2008).
[30] D. Astruc, *Nanoparticles and Catalysis* (Wiley-VCH, Weinheim, 2008).
[31] B. Senyuk, J. S. Evans, P. Ackerman, T. Lee, P. Manna, L. Vigderman, E. R. Zubarev, J. van de Lagemaat, and I. I. Smalyukh, Nano Lett. **12**, 527 (2012).
[32] S. Lal, S. Link, and N. J. Halas, Nat. Photon. **1**, 641 (2007).
[33] J. A. Fan, Ch. Wu, K. Bao, J. Bao, R. Bardhan, N. J. Halas, V. N. Manoharan, P. Nordlander, G. Shvets, and F. Capasso, Science **328**, 1135 (2010).
[34] H. Yoshida, Y. Tanaka, K. Kawamoto, H. Kubo, T. Tsuda, A. Fujii, S. Kuwabata, H. Kikuchi, and M. Ozaki, Appl. Phys. Express **2**, 121501 (2009).

[35] H. Mertens, A. F. Koenderink, and A. Polman, Phys. Rev. B **76**, 115123 (2007).
[36] H. Noh, S. Zelakiewicz, X. G. Feng, T. J. Gramila, L. N. Pfeiffer, and K. W. West, Phys. Rev. B **58**, 12621 (1998).
[37] Q. Liu, B. Senyuk, J. Tang, T. Lee, J. Qian, S. He, and I. I. Smalyukh, Phys. Rev. Lett. **109**, 088301 (2012).
[38] A. J. Morfa, K. L. Rowlen, T. H. Reilly, M. J. Romero, and J. van de Lagemaat, Appl. Phys. Lett. **92**, 013504 (2008).
[39] M. J. Romero and J. van de Lagemaat, Phys. Rev. B **80**, 115432 (2009).
[40] J. C. Johnson, T. H. Reilly, A. C. Kanarr, and J. van de Lagemaat, J. Phys. Chem. C **113**, 6871 (2009).
[41] T. Lee, R. P. Trivedi, and I. I. Smalyukh, Opt. Lett. **35**, 3447 (2010).
[42] D. J. Broer, J. Lub, and G. N. Mol, Nature (London) **378**, 467 (1995).
[43] C. D. Modes and M. Warner, Europhys. Lett. **97**, 36007 (2012).
[44] C. D. Modes and M. Warner, Phys. Rev. E **84**, 021711 (2011).
[45] Y. Sun, J. S. Evans, T. Lee, B. Senyuk, P. Keller, S. He, and I. I. Smalyukh, Appl. Phys. Lett. **100**, 241901 (2012).
[46] B. Senyuk, Q. Liu, S. He, R. D. Kamien, R. B. Kusner, T. C. Lubensky, and I. I. Smalyukh, Nature (London) **493**, 200 (2013).